Chemical and Process Engineering Research
ISSN 2224-7467 (Paper) ISSN 2225-0913 (Online)
Vol.28, 2014

Automated Well Test Analysis I

Ubani C.E and Karl U. Nwala and Onyekonwu M. O

Department of Petroleum Engineering, University of Port-Harcourt

Abstract

Due to the continuous search for cost effective and less time consuming means of obtaining reservoir and well parameters(k, S, etc.), well test analysts have sought for other means of automating the well test interpretation process. Although nonlinear regression is central to the automation process, its use is limited by the subjective selection of the regression reservoir model. This is due to the difficulty in distinguishing the characteristic behavior/features of the pressure (or pressure derivative) response hidden behind noise or of ambiguous plots and this usually leads to wrong parameter estimation. To forestall this problem of model selection, an Artificial Intelligence (AI) approach has been developed to identify the features necessary to discriminate these different models.

This approach completely automates the well test interpretation process and involves the generation of a representative dimensionless pressure derivative data and the extraction of symbolic data from the pressure transient data. This symbolic data is matched with the generated dimensionless pressure derivative data and subsequently used by the AI system to chose the reservoir model and make initial model parameter estimates. Nonlinear regression is then used to refine these estimates. The part 2 of this paper presents the analysis of the results of this approach.

1.0 Introduction

For decades, well tests have been the prime means of estimating reservoir and well parameters (k, S, etc.). However, recent developments in the area of well testing, such as the use of permanent down-hole gauges, call for automated/mechanized model selection and parameter estimation. This is due to the large amount of data acquired and has led to the development and continuous search for other cost effective and less time consuming means of accurately obtaining these parameters.

There are three (***3***) methods of analyzing well test data; *conventional*, *type-curve* and *regression* (or *automated type-curve*) methods (***Onyekonwu***, ***1997***). The conventional method involves using straight lines that are characteristic of the different flow regimes to estimate the desired parameters, while the type-curve method involves finding a type curve that matches the reservoir response, from which the desired parameters can be estimated. The regression or automated type-curve method entails fitting the well test pressure data to an analytical model, from which the required parameters can be estimated. This work is based on the third method, automated type-curve method.

Automated type-curve matching can be seen as a three-stage technique; model selection, initial parameter estimation and regression. The challenges of using regression in well test analysis is compounded by the subjective selection of the regression reservoir model due to the difficulty in distinguishing the characteristic behavior/features of the pressure (or pressure derivative) response hidden behind noise. This usually leads to wrong parameter estimation.

As a solution to this problem, a complete automated well test analysis program that will mechanize all the three stages involved in the regression method is required.

One of the benefits of using non-linear regression is the use of *Confidence Intervals* (***CI***) to measure the goodness of fit. This is used to determine if the appropriate model was selected. As an edge over the conventional and manual type-curve method, nonlinear regression provides the well test analyst a quantitative means of determining how acceptable the parameter estimates are.

1.1 Previous Works

Rosa and ***Horne*** (***1983***) conducted a comprehensive study of nonlinear regression. In the study, they developed techniques that made it relatively easy to implement almost any reservoir model in an automated procedure.

Allain and ***Horne*** (***1990***) used syntactic pattern recognition and a rule-based system to identify the reservoir model by extracting symbolic data from the pressure derivative data. The well and reservoir parameters were also estimated. The limitations of this approach are that it requires a preprocessing of the derivative data in order to distinguish the true response from the noise and a complex definition of rules to accommodate 'nonideal' behavior.

Al-Kaabi and **Lee** (***1990***) used artificial neural networks (ANN) to identify the well test interpretation model from pressure derivative data. Although they reported that this approach was effective in identifying reservoir models and data smoothening was unnecessary, it only provided a qualitative description of the well test. The computation of reservoir parameters was not considered.

Allain and ***Houźe*** (***1992***) presented a hybrid approach to combine the symbolic and artificial neural network methods. In essence, they proposed to use the neural network to determine the sketch of the derivative before applying a rule-based approach to determine the model and estimate its parameters.

Ershaghi et al. (***1993***) implemented multiple neural networks with each neural network representing a single reservoir model. This is to overcome the inefficiency in the training of an enormous number of reservoir models. Although parameter estimation was not mentioned in their work, this approach improved on the shortcomings of the artificial neural network approach as a tool in well test interpretation.

Anraku and ***Horne*** (***1993***) introduced a new approach to discriminate between reservoir models using the *sequential predictive probability* method. This approach was effective in identifying the correct reservoir models by matching to all candidate reservoir models and then computing the probability (joint probability) that each match would correctly predict the pressure response. Candidate reservoir models and initial estimates of the models' parameters need to be determined in advance for this process.

Athichanagorn and ***Horne*** (***1995***) investigated the use of the artificial neural network and the sequential predictive probability approach to recognize characteristic components of candidate models on the derivative plot (unit slope, hump, at slope, dip, and descending shape). This approach was able to discriminate between candidate reservoir models by identifying the flow regimes corresponding to these characteristic components and make initial estimates of their underlying parameters. Nonlinear regression was simultaneously performed on these parameters to compute best estimates of reservoir parameters.

Bariş et al. (***2001***) demonstrated an approach based on Genetic Algorithm (***GA***) with simultaneous regression to automate the entire well test interpretation process. This was able to select the most probable reservoir model among a set of candidate models, consistent with a given set of pressure transient data. They defined the type of reservoir model to be used as a variable type which was estimated together with the other unknown model parameters (permeability, skin, etc.).

Dastan and ***Horne*** (***2011***) made significant improvements to non-linear regression used in well test analysis by developing several different methods to overcome such commonly observed issues such as sensitivity to noise, parameter uncertainty and dependence on starting guesses. The nonlinear techniques regression developed were considered in three groups; the first group involved ***parameter transformations*** (*Cartesian Transform*), the second group, ***data space transformations***, (the *wavelet transform* and *the pressure derivative*) and in the third group, they considered ***alternative objective functions to regular least squares***; *total least squares* (TLS) and *lest absolute value* (LAV). Using these strategies, ***Dastan*** and ***Horne (2011)*** achieved improved performance in terms of likelihood of convergence and narrower confidence intervals (reduced uncertainty), hence making interpretation results more accurate and more stable.

2.0 Objectives and Scope of Work

The objectives of this study are:

1. To present algorithms for data smoothening and for automating the selections of reservoir models in well test analysis.
2. To make an initial estimate of the parameters and refine these estimates using nonlinear regression (Automated Type-Curve Matching).
3. To evaluate the acceptability of the parameter estimates using confidence intervals (***CI***s).

4. To develop a VBA Excel application for automated well test analysis, implementing the above objectives/algorithms.
5. To test the VBA Excel application with simulated and field data and present the results.

The scope of this work is to present a new technique/method for automating well test analysis. This technique is tailored to improve both the performance and accuracy of well test interpretation/analysis and implemented in a computer program, written in Visual Basic programming language. The artificial intelligence (***AI***) approach used in this project is based on the works of ***Allain*** and ***Horne*** (***1990***); with some modifications. This will involve extracting a symbolic representation of the reservoir model from the pressure transient data, estimation of the model parameters from the characteristic flow regimes and subsequently, performing nonlinear regression to refine these parameters. In this research work, eight (**8**) fundamental reservoir models (***Anraku*** and ***Horne***, ***1993***) are used. Namely;

TABLE 1.1: EIGHT FUNDAMENTAL RESERVOIR MODELS

	Reservoir Model	Parameters
1	*Infinite Acting*	K, S, C_s
2	*Sealing Fault*	K, S, C_s, r_e
3	*No flow Outer Boundary*	K, S, C_s, r_e
4	*Constant Pressure Outer Boundary*	K, S, C_s, r_e
5	*Dual Porosity with Pseudosteady State Interporosity Flow*	$K, S, C_s, \omega, \lambda$
6	*Dual Porosity with Pseudosteady State Interporosity Flow and Sealing Fault*	$K, S, C_s, \omega, \lambda, r_e$
7	*Dual Porosity with Pseudosteady State Interporosity Flow and No Flow Outer Boundary*	$K, S, C_s, \omega, \lambda, r_e$
8	*Dual Porosity with Pseudosteady State Interporosity Flow and Constant Pressure Outer Boundary*	$K, S, C_s, \omega, \lambda, r_e$

This work is limited to a single vertical oil well, single layer, as the primary objective of this work is to demonstrate and present the merits of computerizing well test analysis. Although the intervention of a well test analyst is required, this can be greatly minimized by incorporating more complex models, to account for the diverse reservoir configurations, into the program.

The developed program will be tested with 10 data sets. These data sets are generated using a simulator (PanSystem ^{TM}), lifted from literature and actual field data. In nonlinear regression, fitting single rate pressure transient data is as simple as fitting multi-rate pressure transient data, this is one of the benefits of using automated type-curve matching.

3.0 Methodology

The dimensionless pressure derivative plot is a more powerful diagnostic tool, as this makes it easier to identify characteristic features of vague plots. For instance, the plot shown in Figure 3.0.1 could either be a dual-porosity no flow outer boundary or simply a (homogenous) no-flow outer boundary model. This is a clear case of the subjectivity of well test interpretation, as different analysts could have their different justifications for choosing either model. This case is easily solved when the dimensionless pressure derivative plot of the data is analyzed. But the primary challenge is getting a reliable dimensionless pressure derivative plot, as this is a strong function of permeability, *k*. An estimate close to that of Laboratory results could be used in such a case. But this poses a greater problem when such data is not available.

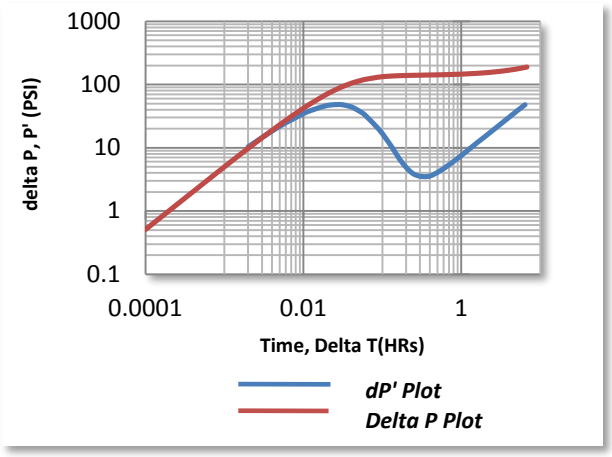

FIGURE 3.0.1: A Typical Ambiguous Diagnostic Plot

This problem was solved by making a rough estimate of permeability, ***k*** and skin, ***S*** from the semi-log plot straight section(s) and regressing on the first few data points using the *infinite acting reservoir model* to get a better estimate (based on the least sum of squares). This permeability, K_{est} is used to evaluate the dimensionless pressure, P_D and dimensionless time, t_D using the following Equations (3.3.7) and (3.3.8).

Using the ***Bourdet et al***. (***1983a***) algorithm, the dimensionless pressure derivative plot is evaluated, smoothened and segmented for model identification. From this a reservoir model is chosen and the model parameters are estimated. The smoothening of noise is imperative as the model identification and parameter estimation algorithms could fail.

This project is implemented using Visual Basic for Applications (VBA) Excel. This chapter describes in detail, all the mathematical tools/algorithms used to implement this methodology. The Methodology workflow is outlined as follows:

- *Log-log Pressure derivative and semi-log pressure data smoothening.*
- *Log-log Pressure derivative and semi-log pressure data segmentation.*
- *Estimation of permeability values from the segmented semi-log straight sections.*
- **Computation of the Dimensionless Pressure derivative using the best 'k' value; based on the least sum-of squares of the regression on the infinite acting model using the first 1.5 cycle of data points.*
- *Dimensionless Pressure derivative data smoothening.*
- *Dimensionless Pressure derivative data segmentation.*
- *Model Identification.*
- *Parameter estimation.*
- *Nonlinear regression.*

3.2 SEGMENTATION ALGORITHM

The algorithm for creating segments of the pressure transient plots is presented in this section. This is based on the works of ***Allain*** and ***Horne*** (***1990***). This is to extract symbolic data which is a representative of the features of the flow regimes.

1. Starting from the first point on the curve, a point is chosen ($\mathbf{x_i}$, $\mathbf{y_i}$) and its slope, $\mathbb{S}^*_i$, with the next adjacent point, ($\mathbf{x_{i+1}}$, $\mathbf{y_{i+1}}$), forms the start of a new segment, $\mathbb{S}_j$.
2. The subsequent immediate point is added to the current segment if its slope, $\mathbb{S}^*_{i+1}$, does not differ by more than a tolerance parameter, ****epsilon*** **(ε),** with the average of the slopes, $\overline{\mathbb{S}^*}_j$, in the segment $\mathbb{SG}_j$. This segment's slope is updated by recalculating the average slope, $\overline{\mathbb{S}^*}_j$.

$$\overline{\mathbb{S}^*}_j = \frac{\sum_{i=1}^{n} \mathbb{S}_i^*}{n} \qquad (3.2.1)$$

* The dual porosity model could be used if a 'MINIMA' is found or if the early time data is truncated. In case of truncated data, the default values for storativity and transmissivity are 0.99 and 1 x 10^{12} respectively.

3. This segment, $\mathbb{SG}_j$, terminates at $(\mathbf{x_n}, \mathbf{y_n})$ with the start of a new segment, $\mathbb{SG}_{j+1}$, where the change in slope is greater than $\boldsymbol{\varepsilon}$, i.e.

$$\overline{\mathbb{S}^*}_j - \mathbb{S}^*_i \geq \varepsilon \tag{3.2.2}$$

4. Each segment, $\mathbb{SG}_j$, will have properties/attributes of ***sg_ft***, **n**,$\overline{\mathbb{S}^*}_j$, $(\mathbf{x}_1, \mathbf{y}_1)$and $(\mathbf{x_n}, \mathbf{y_n})$. W*here:*

sg_ft	*= feature of segment, $\mathbb{SG}_j$.*
$\boldsymbol{n_j}$	*= number of points bound by segment $\mathbb{SG}_j$.*
$(\boldsymbol{x_1}, \boldsymbol{y_1})_j$	*= first point on the segment $\mathbb{SG}_j$.*
$(\boldsymbol{x_n}, \boldsymbol{y_n})_j$	*= last point on the segment $\mathbb{SG}_j$.*
$\overline{\mathbb{S}^*}_j$	*= the average slope of the segment $\mathbb{SG}_j$.*

5. Each segment is compared with the neighbouring segments to identify characteristic features on the plot such as ***extremas*** (*Minimum* and *Maximum*), ***inflexions*** and ***straight sections***.

These features are identified by the AI system using the mathematical expressions presented as follows:

Extremas:

MINIMA

$$\overline{\mathbb{S}^*}_{j-1} < 0 \; and \; \overline{\mathbb{S}^*}_{j+1} > 0 \tag{3.2.3}$$

MAXIMA

$$\overline{\mathbb{S}^*}_{j-1} > 0 \; and \; \overline{\mathbb{S}^*}_{j+1} < 0 \tag{3.2.4}$$

INFLEXION

$$(\overline{\mathbb{S}^*}_{j-1} - \overline{\mathbb{S}^*}_j) \times (\overline{\mathbb{S}^*}_j - \overline{\mathbb{S}^*}_{j+1}) < 0 \tag{3.2.5}$$

STRAIGHT SECTION

A straight section is identified when the number of points, $\mathbf{n_j}$, in the segment, $\mathbb{SG}_j$, exceeds a given minimum, $\mathbf{n_{min}}$, i.e. $\mathbf{n_j} > \mathbf{n_{min}}$.

STEP SECTION

A step section is identified when the number of points, $\mathbf{n_j}$, in the segment, $\mathbb{SG}_j$, is less than a given maximum, $\mathbf{n_{max}}$, i.e. $\mathbf{n_j} < \mathbf{n_{max}}$.

Other segment features for the last segments are ***DOWNTURN*** (if the slope of the last segment falls below a certain negative value), ***UPTURN*** (if the slope of the last segment exceeds a certain positive value) and ***FLAT*** (if the slope is approximately zero).

3.3 BOURDET ET AL. (1983a) PRESSURE DERIVATIVE ALGORITHM

The above expression still results in noise. This can be reduced by selecting data points separated by at least 0.2 of a cycle rather than immediate adjacent points (***Horne, 1995***):

$$t\left(\frac{\partial p}{\partial t}\right)_i = \frac{\ln(t_i/t_{i-k})\Delta P_{i+j}}{\ln(t_{i+j}/t_i)\ln(t_{i+j}/t_{i-k})} + \frac{\ln(t_{i+j}t_{i-k}/t_i^2)\Delta P_i}{\ln(t_{i+j}/t_i)\ln(t_i/t_{i-k})} - \frac{\ln(t_{i+j}/t_i)\Delta P_{i-k}}{\ln(t_i/t_{i-k})\ln(t_{i+1}/t_{i-k})} \tag{3.3.4}$$

$$\ln t_{i+j} - \ln t_i \geq 0.2 \tag{3.3.5}$$

$$\ln t_i - \ln t_{i-k} \geq 0.2 \qquad (3.3.6)$$

The value, 0.2, is known as the differentiation interval and could be replaced with values between 0.1 and 0.5 (***Horne***, ***1995***). This will have different results in the smoothening of the noise.

3.3.1 DIMENSIONLESS PRESSURE DERIVATIVE

Dimensionless pressure drop;

$$P_D = \frac{2\pi kh}{qB\mu}(P_i - P_{wf}) \qquad (3.3.7)$$

Dimensionless time;

$$t_D = \frac{0.000264kt}{\emptyset\mu c_t r_w^2} \qquad (3.3.8)$$

Since the ***Bourdet et al.*** (***1983a***) algorithm is a linear transformation, is can be used to evaluate the dimensionless pressure derivative. Hence, the algorithm is given in terms of dimensionless pressure drop in Equation (3.5.9).

$$t_D\left(\frac{\partial p_D}{\partial t_D}\right)_i = \frac{\ln\left(\frac{t_{D,i}}{t_{D,i-k}}\right)P_{D,i+j}}{\ln\left(\frac{t_{D,i+j}}{t_{D,i}}\right)\ln\left(\frac{t_{D,i+j}}{t_{D,i-k}}\right)} + \frac{\ln\left(\frac{t_{D,i+j}t_{D,i-k}}{t_{D,i}^2}\right)P_{D,i}}{\ln\left(\frac{t_{D,i+j}}{t_{D,i}}\right)\ln\left(\frac{t_{D,i}}{t_{D,i-k}}\right)} - \frac{\ln(t_{D,i+j}/t_{D,i})P_{D,i-k}}{\ln(t_{D,i}/t_{D,i-k})\ln(t_{D,i+1}/t_{D,i-k})} \qquad (3.5.9)$$

3.4 MODEL IDENTIFICATION ALGORITHM

The pseudo-code of the model identification algorithm for the reservoir models used in this work is presented here. This is simplified as this algorithm identifies the models from the segmented dimensionless pressure derivative data. The data segments are looped through as the following pseudo-code identifies the model from the segment 'features'.

MODEL SELECTION PSEUDO-CODE

```
If 'MINIMA' IS present below 0.5 in the SEGMENT collection then
    If last segment feature is 'FLAT' at 1.0 then
        Select Model 6
        Estimate Parameters
    Else if last segment feature is 'UPTURN' then
        Select Model 7
        Estimate Parameters
    Else if last segment feature is 'DOWNTURN' then
        Select Model 8
        Estimate Parameters
    Else
        Select Model 5
        Estimate Parameters

Else if 'MINIMA' IS NOT present or IS present above 0.5 in the SEGMENT collection then
    If last segment feature is 'FLAT' at 1.0 then
```


Select Model 2
Estimate Parameters
Else if last segment feature is 'UPTURN' then
Select Model 3
Estimate Parameters
Else if last segment feature is 'DOWNTURN' then
Select Model 4
Estimate Parameters
Else
Select Model 1
Estimate Parameters

3.5 INITIAL PARAMETER ESTIMATION

The procedures for estimating the model parameters are discussed in this section. These parameters are: *Permeability, Skin, Wellbore Storage Constant, storativity ratio, transmissivity ratio, distance to sealing fault, distance to constant pressure outer boundary and distance to no-flow outer boundary*.

3.5.1 - PERMEABILITY, *k*

The permeability is estimated from the pressure data in the infinite acting period; good transient phase data. This flow regime, on a semi-log plot of pressure versus time (with time on the logarithm scale), is characterized by a straight line. For a drawdown test, the equation describing this straight line is given in Equation (3.5.1).

$$p_{wf} = p_i - 162.6\frac{qB\mu}{kh}\left(\log\ t + \log\frac{k}{\emptyset\mu c_t r_w^2} + 0.8686\,S - 3.2274\right) \quad (3.5.1)$$

where:

p_{wf} = *well flowing pressure, psi*
p_i = *initial reservoir pressure, psi*
μ = *viscosity, cp*
k = *permeability, md*
h = *thickness, ft*
t = *time, hours*
φ = *porosity, dimensionless*
c_t = *total system compressibility, psi*$^{-1}$
r_w = *wellbore radius, ft*
S = *skin factor, dimensionless.*

For a buildup test, this straight line is described by Equation (3.5.2);

$$p_{ws}(\Delta t) = p_i - 162.6\frac{qB\mu}{kh}\log\left(\frac{t_p + \Delta t}{\Delta t}\right) \quad (3.5.2)$$

where:

p_{ws} = *shut-in pressure, psi*
t_p = *producing time, hours*
$\frac{t_p+\Delta t}{\Delta t}$ = *Horner's time, dimensionless*

From the semi-log plot of p_{wf} (or p_{ws}) versus t, the slope, m is used to calculate the value of permeability using Equation (3.5.3).

$$k = \left|162.6\frac{qB\mu}{mh}\right| \quad (3.5.3)$$

3.5.2 - SKIN, *S*

The skin, S, is estimated using equation (3.5.4) which is based on equation (3.5.1).

$$S = 1.151\left(\frac{p_i - p_{1hr}}{m} - \log\frac{k}{\emptyset\mu c_t r_w^2} + 3.2274\right) \quad (3.5.4)$$

If p_{1hr} does not lie on the straight line, the line is extrapolated to t = 1hr, where p_{1hr} is read off.

3.5.3 - WELLBORE **STORAGE CONSTANT, Cs**

The wellbore storage constant is determined using the early time unit slope on the pressure log-log plot. Equation (3.5.5) is used to compute the wellbore storage constant.

$$C_S = \frac{qB \cdot \Delta t}{24 \cdot \Delta P} \quad (3.5.5)$$

Where:

q = production rate, STB/D
B = formation volume factor, res. vol./std vol.
ΔP = pressure drop on the log-log unit slope line, psi
Δt = time at ΔP on the log-log unit slope line, hr

3.5.4 - STORATIVITY RATIO, *ω*

The presence of a dip on a pressure derivative curve suggests reservoir heterogeneity. The storativity ratio (ω) is a dual porosity parameter, which is determined from the minimum point, ($t_D P'_{D,min}$, $t_{D,min}$), on the derivative curve using the procedure described by ***Bourdet et al.*** (***1983b***).

$$t_D\left(\frac{\partial p_D}{\partial t_D}\right)_i = t_D P'_{D,min} = \frac{1}{2}\left(1 + \omega^{\frac{1}{1-\omega}} - \omega^{\frac{\omega}{1-\omega}}\right) \quad (3.5.6)$$

The storativity ratio is evaluated using Equation (3.5.6). But since the relationship between pressure derivative and the storativity ratio is non-linear, the Newton-Raphson's method is used to solve for storativity. The Equations for this procedure are presented as follows:

$$\omega_{new} = \omega_{old} - \frac{f(\omega_{old})}{f'(\omega_{old})} \quad (3.5.7)$$

$$f(\omega) = 1 + \omega^{\frac{1}{1-\omega}} - \omega^{\frac{\omega}{1-\omega}} - 2\,t_D P'_D \quad (3.5.8)$$

and:

$$f'(\omega) = \frac{\ln\omega}{(1-\omega)^2}\left(\omega^{\frac{1}{1-\omega}} - \omega^{\frac{\omega}{1-\omega}}\right) \quad (3.5.9)$$

Equation (3.5.7) is evaluated iteratively until it converges i.e. $\omega_{new} - \omega_{old} \leq \varepsilon$, a small tolerance value.

3.5.5 - TRANSMISSIVITY RATIO, *λ*

The transmissivity ratio (λ) is the second dual porosity parameter, which is also determined from the minimum point, ($t_D P'_{D,min}$, $t_{D,min}$), on the pressure derivative curve using the procedure described by ***Bourdet et al.*** (***1983b***).The transmissivity ratio (λ) is evaluated using Equation (3.5.11).

$$t_{D,min} = \frac{\omega}{\lambda} ln\frac{1}{\omega} \quad (3.5.10)$$

Hence,

$$\lambda = \frac{\omega}{t_{D,min}} ln\frac{1}{\omega} \quad (3.5.11)$$

3.5.6 - DISTANCE TO BOUNDARY, r_e

For buildup tests, there is no distinct feature for determining the boundary type; the pressure derivative decreases irrespective of the type of boundary reached by the pressure transient. Thus, the distance to boundary for any boundary type is estimated using the radius of investigation, ***r_{inv} (Lee, 1982)***.

$$r_{inv} = \sqrt{\frac{4 \times 0.000264\, \mathrm{k\,t}}{\emptyset \mu c_t r_w^2}} \qquad (3.5.12)$$

Where;

t, is the time the pressure derivative starts to decrease or the end of the test if the boundary has not been reached.

The distance to boundary for drawdown tests can be determined for the following boundary types as follows:

a) DISTANCE TO SEALING FAULT

The presence of an 'upward' trend followed by a 'flat' at late time on a dimensionless pressure derivative plot at 1.0 indicates the presence of a sealing fault. With this, a doubling of slope on the semi-log plot, which is also indicative of the presence of a sealing fault, is used to compute the distance to sealing fault boundary (***d***). ***Davis*** and ***Hawkins*** (***1963***) and ***Gray*** (***1965***) described how to evaluate the distance to the fault boundary using the time, t_x where the two straight lines intersect on the semilog plot.

$$d = \sqrt{\frac{1.48 \times 10^{-4}\, \mathrm{k\,t_x}}{\emptyset \mu c_t}} \qquad (3.5.13)$$

b) DISTANCE TO CONSTANT PRESSURE OUTER BOUNDARY

When a constant pressure boundary is reached by the pressure transient, the reservoir encounters a steady state flow regime. This is indicated by a steady decrease of the pressure derivative and a constant pressure at the well. The dimensionless pressure drop (P_D) can be expressed as follows:

$$P_D = ln\frac{r_e}{r_w} \qquad (3.5.14)$$

Taking the dimensionless pressure drop to include the skin, Equation (3.5.14) can be substituted in to Equation (3.3.7) as follows:

$$\frac{kh}{141.2\, qB\mu}(p_i - p_{wf}) + S = ln \qquad (3.5.15)$$

Therefore the distance to the constant pressure boundary, $\mathbf{r_e}$ can be calculated as follows:

$$r_e = r_w\, e^{\frac{kh}{141.2\, qB\mu}(p_i - p_{wf}) - S} \qquad (3.5.16)$$

c) DISTANCE TO NO-FLOW OUTER BOUNDARY

The distance to a closed boundary can be estimated from the pressure data in the pseudo-steady state flow period. During this period, the pressure change is a linear function of time as described by Equation (3.5.17):

$$p_i - p_{wf} = \frac{0.2342 qB}{\phi c_t hA} t + 70.65 \frac{qB\mu}{kh}(\ln(2.2458 A C_A r_w^2) + 2\,S) \qquad (3.5.17)$$

where;

A = reservoir area, ft^2
C_A = shape factor, dimensionless

From the slope of the Cartesian straight line, $m_{Cartesian}$, the drainage area can be calculated using:

$$A = \frac{0.2342qB}{\phi c_t h\, m_{Cartesian}} \tag{3.5.18}$$

Assuming a circular reservoir, the distance to the boundary, $\mathbf{r_e}$ can be calculated using:

$$r_e = \sqrt{\frac{A}{\pi}} \tag{3.5.19}$$

3.6 RESERVOIR MODELS

The eight (***8***) fundamental reservoir models (***Anraku***, ***1993***) used in this work are described in this section***; Infinite Acting, Sealing Fault, No flow Outer Boundary, Constant Pressure Outer Boundary, Dual Porosity with Pseudosteady State Interporosity Flow, Dual Porosity with Pseudosteady State Interporosity Flow and Sealing Fault, Dual Porosity with Pseudosteady State Interporosity Flow and No Flow Outer Boundary and Dual Porosity with Pseudosteady State Interporosity Flow*** and ***Constant Pressure Outer Boundary***. Characteristic plots and the governing equations of these reservoir models are presented in this section. Although, the analytical derivatives of pressure drop with the model parameters were used in performing nonlinear regression, they will not be presented in this work. Interested readers should refer to ***Anraku*** (***1993***) for the analytical derivatives of pressure drop with model parameters.

$$\eta = \frac{k}{\emptyset \mu c_t} \tag{3.6.1}$$

$$c_1 = \frac{h}{141.2\mu} \tag{3.6.2}$$

$$\Delta P = (P_i - P_w) \tag{3.6.3}$$

3.6.1 - INFINITE ACTING MODEL

The Infinite Acting Model has three (***3***) parameters; k, S and C_s. A typical plot of this model is shown in FIGURE 3.6.1; this is a simulated plot of the infinite acting model using a ***k*** of 920.844mD, ***S*** of 24.669 and $\boldsymbol{C_s}$ of 0.01 bbl/psi. On the pressure derivative plot, this model is characterized by a flat at late time.

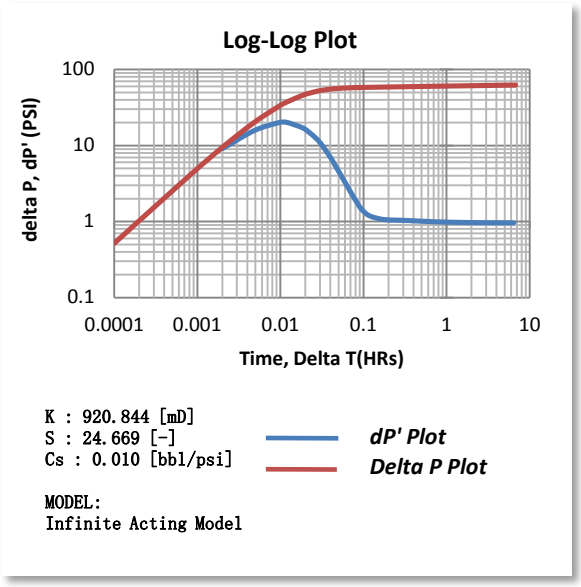

FIGURE 3.6.1: Infinite Acting Model – Simulated using 'Well Test Auto'

The pressure drop at the wellbore for the infinite acting model in field units is given in Laplace space as;

$$\overline{\Delta p} = \frac{qB}{z}.\frac{A_1}{A_2} \qquad (3.6.4)$$

$$u = \frac{r_w^2}{0.000264\eta}\cdot z \qquad (3.6.5)$$

Where:

$$A_1 = K_0(\sqrt{u}) + S\sqrt{u}K_1(\sqrt{u}) \qquad (3.6.6)$$

$$A_2 = c_1 k\sqrt{u}K_1(\sqrt{u}) + 24Cz.A_1 \qquad (3.6.7)$$

When skin, S is negative, the concept of the effective radius is used to avoid numerical instabilities as follows;

$$r_{weff} = r_w e^{-s} \qquad (3.6.8)$$

$$u = \frac{r_{weff}^2}{0.000264\eta}\cdot z \qquad (3.6.9)$$

$$A_1 = K_0(\sqrt{u}) \qquad (3.6.11)$$

Where: r_{weff} is the effective radius of the wellbore.

3.6.2- SEALING FAULT MODEL

The sealing fault model has four (4) parameters; k, S, C_s and r_e. A typical plot of this model is shown in FIGURE 3.6.2; this is a simulated plot using a ***k*** of 920.00mD, ***S*** of 24.0, C_s of 0.01 bbl/psi and r_e of 1200.00ft. On the pressure derivative plot, this model is characterized by an upward trend followed by a flat at late time.

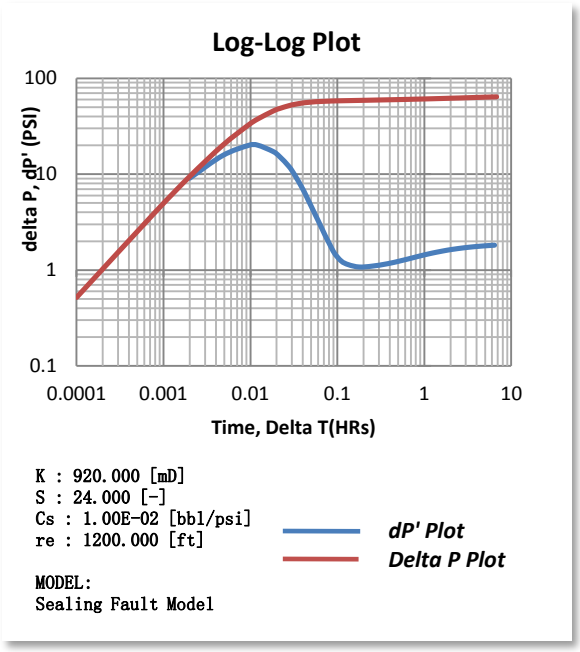

FIGURE 3.6.2: Sealing Fault Model – Simulated using 'Well Test Auto'

The pressure drop at the wellbore for the sealing fault model in field units is given in Laplace space as;

$$\overline{\Delta p} = \frac{qB}{z}.\frac{A_1}{A_2} \qquad (3.6.11)$$

$$w = \frac{4r_e^2}{0.000264\eta}z \qquad (3.6.12)$$

$$u = \frac{r_w^2}{0.000264\eta}z \qquad (3.6.13)$$

where:

$$A_1 = A_{11} + A_{12} \qquad (3.6.14)$$

$$A_{11} = K_0(\sqrt{u}) + S\sqrt{u}K_1(\sqrt{u}) \qquad (3.6.15)$$

$$A_{12} = K_0(\sqrt{w}) \qquad (3.6.16)$$

$$A_2 = c_1 k\sqrt{u}K_1(\sqrt{u}) + 24Cz \cdot A_{11} \qquad (3.6.17)$$

When skin, S, is negative, the concept of the effective radius is used to avoid numerical instabilities. Equation (3.6.8) and (3.6.9) are used to calculate the effective radius, $\boldsymbol{r_{weff}}$ and reevaluate $\boldsymbol{u}$;

and :

$$A_{11} = K_0(\sqrt{u}) \qquad (3.6.18)$$

3.6.3 - NO FLOW OUTER BOUNDARY MODEL

The no-flow outer boundary model has four (4) parameters; k, S, C_s and r_e. A typical plot of this model is shown in FIGURE 3.6.3; this is a simulated plot using a $\boldsymbol{k}$ of 920.44mD, $\boldsymbol{S}$ of 24.669, $\boldsymbol{C_s}$ of 0.01 bbl/psi and $\boldsymbol{r_e}$ of 1200.00ft. On the pressure derivative plot, this model is characterized by an upward trend at late time.

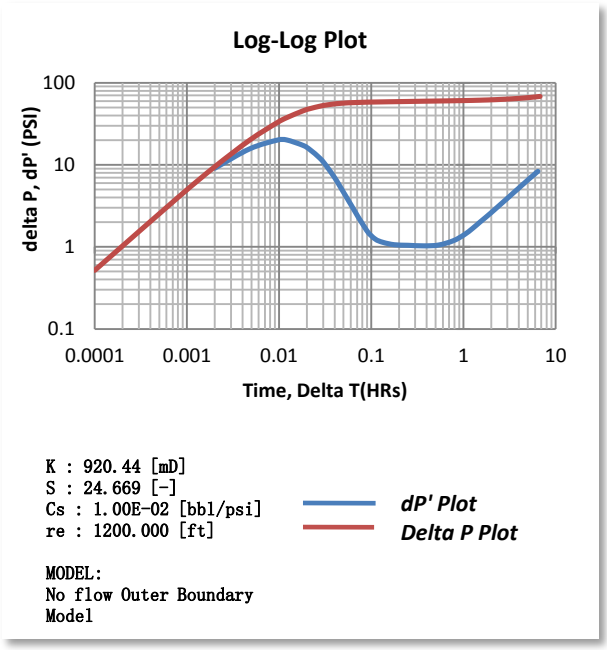

FIGURE 3.6.3: No Flow Outer Boundary Model– Simulated using 'Well Test Auto'

The pressure drop at the wellbore for the no-flow outer boundary model in field units is given in Laplace space as;

$$\overline{\Delta p} = \frac{qB}{z} \cdot \frac{A_1}{A_2} \qquad (3.6.19)$$

$$w = \frac{r_e^2}{0.000264\eta} \cdot z \qquad (3.6.20)$$

$$u = \frac{r_w^2}{0.000264\eta} \cdot z \qquad (3.6.21)$$

where:

$$A_1 = B_1 + S\sqrt{u} \cdot B_2 \qquad (3.6.22)$$

$$B_1 = I_1(\sqrt{w})K_0(\sqrt{u}) + K_1(\sqrt{w})I_0(\sqrt{u}) \qquad (3.6.23)$$

$$B_2 = I_1(\sqrt{w})K_1(\sqrt{u}) - K_1(\sqrt{w})I_1(\sqrt{u}) \qquad (3.6.24)$$

$$A_2 = c_1 k\sqrt{u}B_2 + 24Cz.A_1 \qquad (3.6.25)$$

When skin, S, is negative, the concept of the effective radius is used by calculating the effective radius, $\boldsymbol{r_{weff}}$ and reevaluating $\boldsymbol{u}$ using Equation (3.6.8) and (3.6.9) respectively;

and :

$$A_1 = B_1 \qquad (3.6.26)$$

3.6.4 - CONSTANT PRESSURE OUTER BOUNDARY MODEL

The constant pressure outer boundary model has four (***4***) parameters; k, S, C_s and r_e. A typical plot of this model is shown in FIGURE 3.6.4; this is a simulated plot using a ***k*** of 920.844mD, ***S*** of 24.669, $\boldsymbol{C_s}$ of 0.01 bbl/psi and $\boldsymbol{r_e}$ of 800.00ft. This model is characterized by a downward trend at late time. On the pressure derivative plot, this model is characterized by a downward trend at late time.

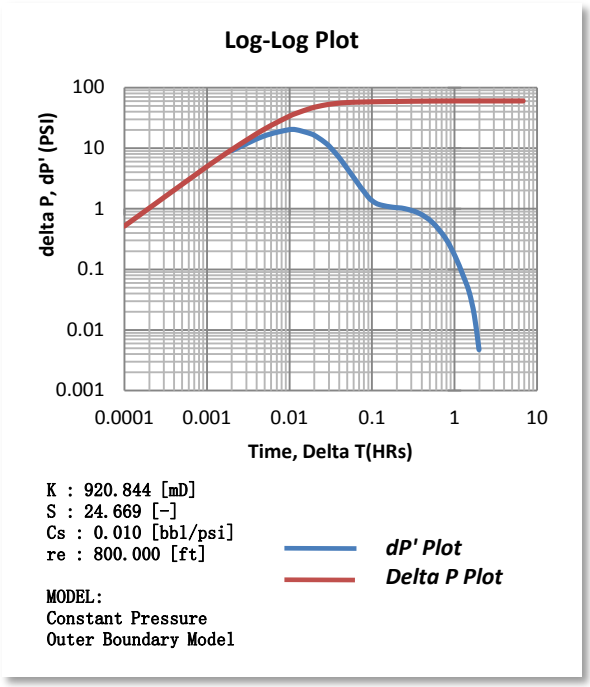

FIGURE 3.6.4: Constant Pressure Outer Boundary Model– Simulated using 'Well Test Auto'

The pressure drop at the wellbore for the constant pressure outer boundary model in field units is given in Laplace space as;

$$\overline{\Delta p} = \frac{qB}{z} \cdot \frac{A_1}{A_2} \qquad (3.6.27)$$

$$w = \frac{r_e^2}{0.000264\eta} \cdot z \qquad (3.6.28)$$

$$u = \frac{r_w^2}{0.000264\eta} \cdot z \qquad (3.6.29)$$

where:

$$A_1 = B_3 + S\sqrt{u} \cdot B_4 \qquad (3.6.30)$$

$$B_3 = I_0(\sqrt{w})K_0(\sqrt{u}) - K_0(\sqrt{w})I_0(\sqrt{u}) \qquad (3.6.31)$$

$$B_2 = I_0(\sqrt{w})K_1(\sqrt{u}) + K_0(\sqrt{w})I_1(\sqrt{u}) \qquad (3.6.32)$$

$$A_2 = c_1 k\sqrt{u} \cdot B_4 + 24Cz.A_1 \qquad (3.6.33)$$

When skin, S, is negative, the concept of the effective radius is used by calculating the effective radius, $\boldsymbol{r_{weff}}$ and reevaluating $\boldsymbol{u}$ using Equation (3.6.8) and (3.6.9) respectively;

and :

$$A_1 = B_3 \qquad (3.6.34)$$

3.6.5 - DUAL POROSITY MODEL

The dual porosity model has four (5) parameters; k, S, C_s, ω and λ. A typical plot of this model is shown in FIGURE 3.6.5; this is a simulated plot using a ***k*** of 889.64mD, ***S*** of 23.629, $\boldsymbol{C_s}$ of 0.00996 bbl/psi, **ω** of 0.05 and $\boldsymbol{\lambda}$ of 2.0 x 10^{-6}. This model is characterized by a dip at middle time on the pressure derivative plot.

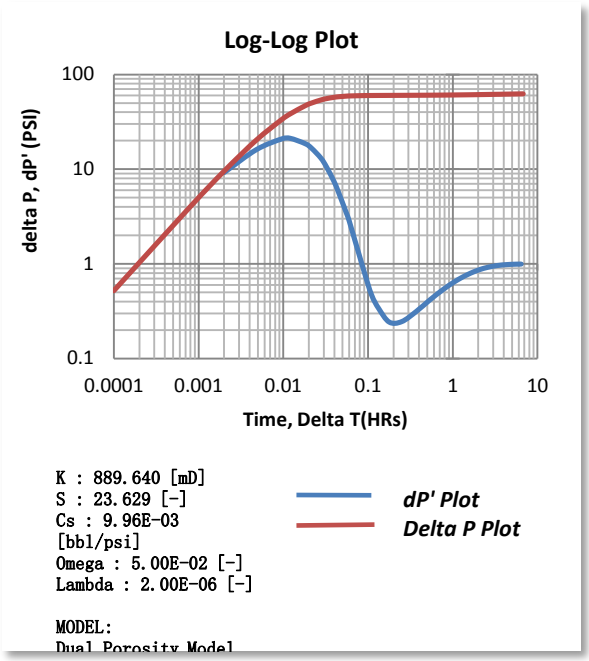

FIGURE 3.6.5: Dual Porosity Model – Simulated using 'Well Test Auto'

The pressure drop at the wellbore for the dual porosity model in field units is given in Laplace space as;

$$\overline{\Delta p} = \frac{qB}{z}.\frac{A_1}{A_2} \qquad (3.6.35)$$

$$v = u \cdot \frac{w(1-w)u + \lambda}{(1-w)u + \lambda} \qquad (3.6.36)$$

$$u = \frac{r_w^2}{0.000264\eta} z \qquad (3.6.37)$$

Where:

$$A_1 = K_0(\sqrt{v}) + S\sqrt{v}K_1(\sqrt{v}) \qquad (3.6.38)$$

$$A_2 = c_1 k\sqrt{v}K_1(\sqrt{v}) + 24Cz.A_1 \qquad (3.6.39)$$

When skin, S, is negative, the concept of the effective radius is used by calculating the effective radius, $\boldsymbol{r_{weff}}$ and reevaluating ***u*** using Equation (3.6.8) and (3.6.9) respectively;

and :

$$A_1 = K_0(\sqrt{v}) \qquad (3.6.40)$$

3.6.6 - DUAL POROSITY AND SEALING FAULT MODEL

The dual porosity and sealing fault model has six (6) parameters; k, S, C_s, ω, λ and r_e. A typical plot of this model is shown in FIGURE 3.6.6; this is a simulated plot using a ***k*** of 889.64mD, ***S*** of 23.629, $\boldsymbol{C_s}$ of 0.00996 bbl/psi, **ω** of 0.05, $\boldsymbol{\lambda}$ of 2.0 x 10^{-6} and r_e of 1300.00ft. On the pressure derivative plot, this model is characterized by a dip at middle time and an upward trend followed by a flat at late time.

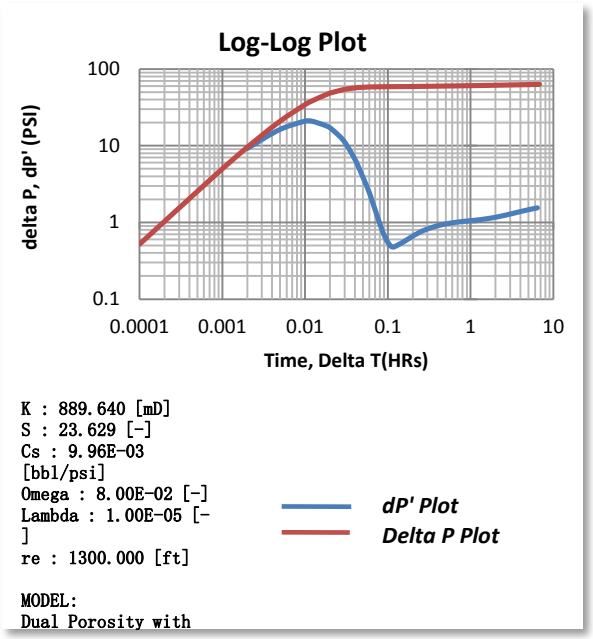

FIGURE 3.6.6: Dual Porosity with Sealing Fault Model – Simulated using 'Well Test Auto'

The pressure drop at the wellbore for the dual porosity sealing with fault model in field units is given in Laplace space as;

$$\overline{\Delta p} = \frac{qB}{z}.\frac{A_1}{A_2} \tag{3.6.41}$$

$$v = u \cdot \frac{w(1-w)u + \lambda}{(1-w)u + \lambda} \tag{3.6.42}$$

$$w = \frac{4r_e^2}{r_w^2} \cdot v \tag{3.6.43}$$

$$u = \frac{r_w^2}{0.000264\eta} z \tag{3.6.44}$$

where:

$$A_1 = B_1 + B_2 \tag{3.6.45}$$

$$B_1 = K_0(\sqrt{v}) + S\sqrt{v}K_1(\sqrt{v}) \tag{3.6.46}$$

$$B_2 = K_0(\sqrt{w}) \tag{3.6.47}$$

$$A_2 = c_1 k\sqrt{v}K_1(\sqrt{v}) + 24Cz \cdot A_1 \tag{3.6.48}$$

When skin, S, is negative, the concept of the effective radius is used by calculating the effective radius, $\boldsymbol{r_{weff}}$ and reevaluating $\boldsymbol{u}$ using Equation (3.6.8) and (3.6.9) respectively;

and :

$$B_1 = K_0(\sqrt{v}) \qquad (3.6.49)$$

3.6.7 - DUAL POROSITY NO FLOW OUTER BOUNDARY MODEL

The dual porosity no-flow outer boundary model has six (6) parameters; k, S, C_s, ω, λ and r_e. A typical plot of this model is shown in FIGURE 3.6.7; this is a simulated plot using a ***k*** of 920.00mD, ***S*** of 25.00, $\boldsymbol{C_s}$ of 0.01

bbl/psi, **ω** of 0.01, λ of 7.0 x 10^{-7} and r_e of 800.00ft. On the pressure derivative plot, this model is characterized by a dip at middle time and an upward trend at late time.

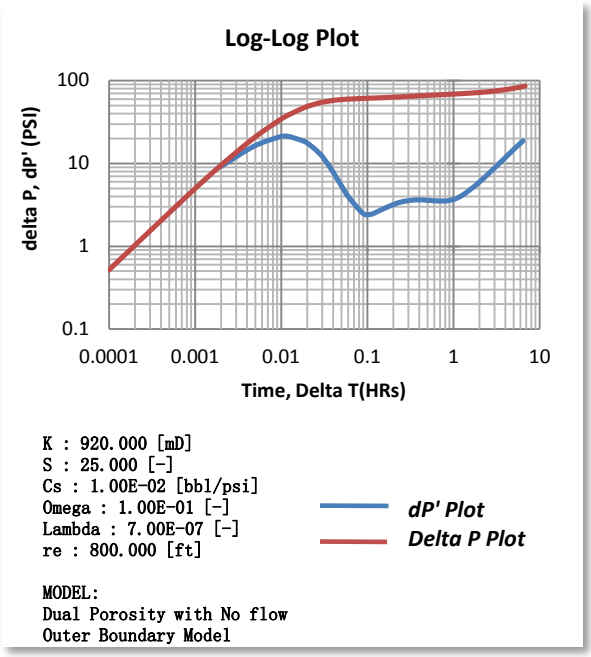

FIGURE 3.6.7: Dual Porosity with No Flow Outer Boundary Model – Simulated using 'Well Test Auto'

The pressure drop at the wellbore for the dual porosity with no-flow outer boundary model in field units is given in Laplace space as;

$$\overline{\Delta p} = \frac{qB}{z} \cdot \frac{A_1}{A_2} \tag{3.6.50}$$

$$v = u \cdot \frac{w(1-w)u + \lambda}{(1-w)u + \lambda} \tag{3.6.51}$$

$$w = \frac{r_e^2}{r_w^2} \cdot v \tag{3.6.52}$$

$$u = \frac{r_w^2}{0.000264\eta} \cdot z \tag{3.6.53}$$

Where:

$$A_1 = B_1 + S\sqrt{v} \cdot B_2 \tag{3.6.54}$$

$$B_1 = I_1(\sqrt{w})K_0(\sqrt{v}) + K_1(\sqrt{w})I_0(\sqrt{v}) \tag{3.6.55}$$

$$B_2 = I_1(\sqrt{w})K_1(\sqrt{v}) - K_1(\sqrt{w})I_1(\sqrt{v}) \tag{3.6.56}$$

$$A_2 = c_1 k\sqrt{u} \cdot B_2 + 24Cz.A_1 \tag{3.6.57}$$

When skin, S, is negative, the concept of the effective radius is used by calculating the effective radius, $\boldsymbol{r_{weff}}$ and reevaluating $\boldsymbol{u}$ using Equation (3.6.8) and (3.6.9) respectively;

and:

$$A_1 = B_1 \tag{3.6.58}$$

3.6.8 - DUAL POROSITY CONSTANT PRESSURE OUTER BOUNDARY MODEL

The dual porosity constant pressure outer boundary model has six (6) parameters; k, S, C_s, ω, λ and r_e. A typical plot of this model is shown in FIGURE 3.6.8; this is a simulated plot using a ***k*** of 889.64mD, ***S*** of 23.629, $\boldsymbol{C_s}$ of 0.00996 bbl/psi, **ω** of 0.05, $\boldsymbol{\lambda}$ of 1.0 x 10^{-5} and r_e of 1000.00ft. On the pressure derivative plot, this model is characterized by a dip at middle time and a downward trend at late time.

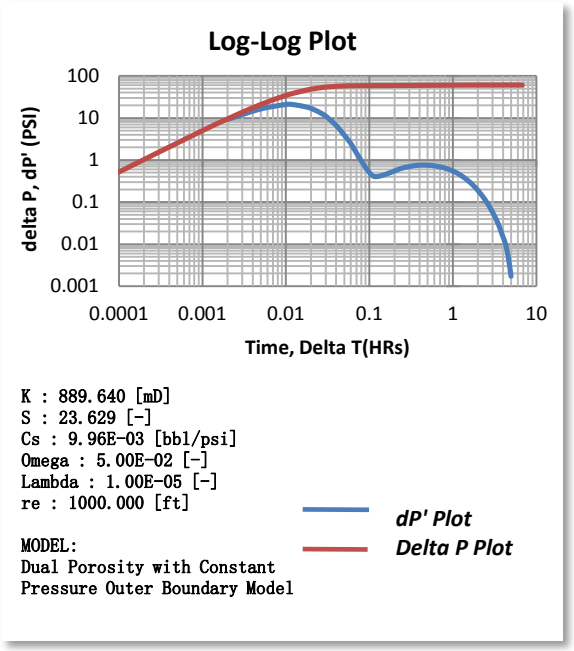

FIGURE 3.6.8: Dual Porosity with Constant Pressure Outer Boundary Model – Simulated using 'Well Test Auto'

The pressure drop at the wellbore for the dual porosity with constant pressure model in field units is given in Laplace space as;

$$\overline{\Delta p} = \frac{qB}{z} \cdot \frac{A_1}{A_2} \qquad (3.6.59)$$

$$v = u \cdot \frac{w(1-w)u + \lambda}{(1-w)u + \lambda} \qquad (3.6.60)$$

$$w = \frac{r_e^2}{r_w^2} \cdot v \qquad (3.6.61)$$

$$u = \frac{r_w^2}{0.000264\eta} \cdot z \qquad (3.6.62)$$

where:

$$A_1 = B_3 + S\sqrt{v} \cdot B_4 \qquad (3.6.63)$$

$$B_3 = I_0(\sqrt{w})K_0(\sqrt{v}) - K_0(\sqrt{w})I_0(\sqrt{v}) \qquad (3.6.64)$$

$$B_2 = I_0(\sqrt{w})K_1(\sqrt{v}) + K_0(\sqrt{w})I_1(\sqrt{v}) \quad (3.6.65)$$

$$A_2 = c_1 k\sqrt{v} \cdot B_4 + 24Cz.A_1 \quad (3.6.66)$$

When skin, S, is negative, the concept of the effective radius is used by calculating the effective radius, r_{weff} and reevaluating u using Equation (3.6.8) and 3.6.9 respectively;

and:

$$A_1 = B_3 \quad (3.6.67)$$

3.7 STEHFEST'S ALGORITHM

This is a numerical Laplace inverse technique, first introduced by Graver and its algorithm presented by ***Stehfest*** (***1970***). This method is extensively used in petroleum engineering literature because of its simplicity and ease of implementation. The algorithm uses the following equation to approximate the time domain;

$$f(t) = \frac{ln2}{t} \cdot \sum_{i=1}^{n} V_i F\left(\frac{ln2}{t} \cdot i\right) \quad (3.7.1)$$

Where the Stehfest's Coefficient, V_i is computed as follows;

$$V_i = (-1)^{\left(\frac{n}{2}+1\right)} \sum_{k_1=\left(\frac{i+1}{2}\right)}^{\min\left(i,\frac{n}{2}\right)} \frac{k_1^{\left(\frac{n}{2}+1\right)}(2k}{\left(\frac{n}{2}+k_1\right)!\,k_1!\,(i-k_1} \quad (3.7.2)$$

And ***n,*** is a heuristic integral parameter which represents the number of terms used in the summation in Equation (3.7.1). An optimal choice of $10 \leq n \leq 14$ has been commonly observed.

3.8 BESSEL FUNCTIONS

The modified Bessel functions of the of integer order, $I_n(x)$ and $K_n(x)$ are used in this work; where ***n*** is the order of the Bessel function. For the reservoir models used in this work, the modified Bessel functions of the first and second kind and of zero and first order are evaluated based on polynomial coefficients given by ***Abromowitz*** and ***Stegun*** (***1964***).

3.9 NONLINEAR REGRESSION

3.9.1 - LEVENBERG-MARQUARDT ALGORITHM

The Levenberg-Marquardt algorithm (***LMA***), also called the *Marquardt method*, is a very popular numerical solution to the problem of minimizing a function (generally nonlinear) over a space of parameters of the function; *nonlinear regression*. In a nutshell, the LMA is a solution to the least squares curve fitting problem. This algorithm interposes between the gradient decent algorithm and the Gauss-Newton algorithm. Although the LMA tends to be a bit slower than the Gauss-Newton algorithm (GNA), it is more robust than the GNA i.e. in most cases the LMA finds a solution even if it starts far off the final minimum. However, the LMA algorithm only finds local minima, instead of the required global minima.

In nonlinear regression, given a set of ***N*** empirical datum pairs of independent and dependent variables, (t_i, p_i), with model parameters ***a,*** the LMA seeks to minimize the sum of squares of the deviations; the objective function, *E* (***a***);

$$E(\boldsymbol{a}) = \sum_{i}^{N} (p(t_i; \boldsymbol{a}) - p_i)^2, \tag{3.9.1}$$

by optimizing the parameters ***a*** of the model curve, ***p(t_i; a)***.

Therefore, LMA is a curve fitting algorithm for a model which depends nonlinearly on the set of unknown parameters $\boldsymbol{a_k}$, $\boldsymbol{k}$ = 1, 2, …, M. A merit function $\boldsymbol{\chi^2}$ is defined and its minimization is used to determine best-fit parameters $\boldsymbol{a}$*. Hence, the merit function is the objective function of this minimization problem. This nonlinear dependency implies that minimization must proceed iteratively. This procedure aims to improve the initial trail values of the fit parameters $\boldsymbol{a_0}$.

With the model function;

$$p = p(t; a), \tag{3.9.2}$$

the chi-square χ^2 merit function can be defined as;

$$\boldsymbol{\chi^2}(\boldsymbol{a}) = \sum_{i=1}^{N} [p_i - p(t_i; a)]^2 \tag{3.9.3}$$

The Taylor's series expansion of a function, *f(x)* is expressed as;

$$f(x) = f(x_0) + (x - x_0)\frac{\partial f}{\partial x} + \frac{(x - x_0)^2}{2}\frac{\partial^2 f}{\partial x^2} + \cdots \tag{3.9.4}$$

In matrix notation ($A = \frac{\partial^2 f}{\partial x^2}$), *f(x)* is expressed as;

$$f(x) \cong f(x_0) + (x - x_0) \cdot \nabla f(x) + \frac{1}{2}(x - x_0) \cdot A \cdot (x - x_0) \tag{3.9.5}$$

$$\therefore if, \quad f(x) \equiv E(a) \equiv \chi^2(a), \tag{3.9.6}$$

then, as the objective function converges,

$$f(x) - f(x_0) \to 0 \tag{3.9.7}$$

Substituting this into Equation (3.9.4) and dividing through by $(x - x_0)$, results in Equation (3.9.8) i.e. in matrix notation;

$$\nabla f(x) + \frac{1}{2} \cdot A \cdot (x - x_0) = 0 \tag{3.9.8}$$

$$\therefore x = x_0 - \mathrm{A}^{-1} \cdot \nabla f(x_0) \tag{3.9.9}$$

Similarly, our objective function, $\chi^2(\boldsymbol{a})$ can be expressed as follows, using Taylor's series expansion;

$$\boldsymbol{\chi}(\boldsymbol{a}) = \chi(a_0) + (a - a_0)\frac{\partial \chi^2}{\partial a} + \frac{1}{2} \cdot (a - a_0)^2 \frac{\partial^2 \chi^2}{\partial a^2} + \cdots \tag{3.9.10}$$

$$\therefore \; a_{next} = a_{cur} + \mathrm{A}^{-1} \cdot [-\nabla \chi^2(a_{cur})] \tag{3.9.11}$$

The first partial derivative of the merit function, $\boldsymbol{\chi^2}$ with respect to the model parameters is given as;

$$\frac{\partial \chi^2}{\partial a_k} = -2\sum_{i=1}^{N}[p_i - p(t_i;a)]\cdot\frac{\partial p(t_i,a)}{\partial a_k} \qquad (3.9.12)$$

Taking additional partial derivatives (the Hessian matrix),

$$\frac{\partial^2 \chi^2}{\partial a_k \partial a_l} = 2\sum_{i=1}^{N}\left[\frac{\partial p(t_i;a)}{\partial a_k}\frac{\partial p(t_i;a)}{\partial a_l} - [p_i - p(t_i;a)]\frac{\partial^2 p(t_i;a)}{\partial a_l \partial a_k}\right] \qquad (3.9.13)$$

Let α and β be defined as follows;

$$\beta_k = -\frac{1}{2}\frac{\partial \chi^2}{\partial a_k} \qquad (3.9.14)$$

$$\alpha_{kl} = \frac{1}{2}\frac{\partial^2 \chi^2}{\partial a_k \partial a_l} \qquad (3.9.15)$$

$$\alpha_{kl} \cong \sum_{i=1}^{N}\left[\frac{\partial p(t_i;a)}{\partial a_k}\frac{\partial p(t_i;a)}{\partial a_l}\right] \qquad (3.9.16)$$

$$\sum_{l=1}^{M}\alpha_{kl}\delta a_l = \beta_k \qquad (3.9.17)$$

where : δa = parameter increment

Levenberg proposed the introduction of a non-negative dampening factor λ, as shown in Equation 3.9.18. This dampening factor, λ, is adjusted at each iteration step, with a smaller value of λ used if there is a reduction in χ^2 and vice versa.

$$\alpha_{kl}' \equiv \alpha_{kl}(1 + \lambda) \qquad (3.9.18)$$

$$\sum_{l=1}^{M}\alpha_{kl}'\delta a_l = \beta_k \qquad (3.9.19)$$

Marquardt later provided the insight of diagonal scaling to improve convergence over small gradients. This improvement is shown in Equation (3.9.20) and (3.9.21) as a modification to Equation (3.9.18). This is bases of the Levenberg-Marquardt algorithm.

$$\alpha_{jj}'' \equiv \alpha_{jj}(1 + \lambda) \qquad (3.9.20)$$

$$\alpha_{jk}'' \equiv \alpha_{jk} \qquad (j \neq k) \qquad (3.9.21)$$

$$\sum_{l=1}^{M}\alpha_{kl}''\delta a_l = \beta_k \qquad (3.9.22)$$

Given an initial guess for the set of fitted parameters $\boldsymbol{a_0}$, ***Press et al.*** (***2007***) briefly outlined the LMA steps as follows:

1. *Compute $\chi^2(\boldsymbol{a})$.*
2. *Pick a modest value for λ, say $\lambda = 0.001$.*
3. *Solve the linear equations (Equation* 3.9.22*) for $\delta\boldsymbol{a}$ and evaluate $\chi^2(\boldsymbol{a}+\delta\boldsymbol{a})$.*
4. *If $\chi^2(\boldsymbol{a}+\delta\boldsymbol{a}) \geq \chi^2(\boldsymbol{a})$, increase λ by a factor of 10 (or any other substantial factor) and go back to (3).*
5. *If $\chi^2(\boldsymbol{a}+\delta\boldsymbol{a}) < \chi^2(\boldsymbol{a})$, decrease λ by a factor of 10, update the trial solution $\boldsymbol{a} = \boldsymbol{a} + \delta\boldsymbol{a}$, and go back to (3).*

A tolerance value $\boldsymbol{\varepsilon}$ of $\chi^2(\boldsymbol{a}+\delta\boldsymbol{a}) - \chi^2(\boldsymbol{a})$ is set as a stopping condition i.e. convergence criteria . Alternatively, the maximum number of iterations can be set as a stopping condition. A reasonable value of $\boldsymbol{\varepsilon}$ is chosen, so as to avoid unnecessary and wasteful computation time. To test for convergence, the merit function χ^2 used in steps 4 and 5 is combined with the pressure derivative data as follows;

$$\boldsymbol{\chi^2(a)} = 0.5 \times \sum_{i=1}^{N'} [p_i - p(t_i; a)]^2 + 0.5 \times \sum_{i=1}^{N'} \left[p'_i - p'(t_i; a)\right]^2 \qquad (3.9.23)$$

Where; p'_i = the pressure derivative data at time t_i.
N' = the number of pressure derivative data points.

This is to improve the convergence of dual porosity models.
The ***Barrier method*** was used to constrain the parameter estimates. This was done by setting upper (***UB***) and lower bounds (***LB***) of the parameters. In implementing this method, a parameter is only updated after an iteration step if it falls within the bounds i.e. between UB and LB.

If $(\boldsymbol{a}+\delta\boldsymbol{a}) \leq \boldsymbol{UB}$ and $(\boldsymbol{a}+\delta\boldsymbol{a}) \geq \boldsymbol{LB}$ then
Update the parameter, $\boldsymbol{a} = \boldsymbol{a}+\delta\boldsymbol{a}$
Else $\boldsymbol{a} = \boldsymbol{a}$

The upper and lower parameter bounds were set from the initial estimates as presented in table 3.9.1.

The linear equations (Equation 3.9.22) are solved using ***Gaussian elimination method***. ***Press et al.*** (***2007***) presented, in detail, the implementation of ***Gaussian elimination method***.

TABLE 3.9.1: UPPER AND LOWER LIMITS

Parameter	*UB*	*LB*
$\boldsymbol{K}$	K_{est} +*10%* of K_{est}	K_{est} - *10%* of K_{est}
$\boldsymbol{C_s}$	$C_{s,est}$ +*10%* of $C_{s,est}$	$C_{s,est}$ - *10%* of $C_{s,est}$
$\boldsymbol{\omega}$	ω_{est} +*10%* of ω_{est}	ω_{est} - *10%* of ω_{est}
$\boldsymbol{\lambda}$	λ_{est} +*10%* of λ_{est}	λ_{est} - *10%* of λ_{est}
$\boldsymbol{r_e}$	$r_{e,est}$ +*10%* of $r_{e,est}$	$r_{e,est}$ - *10%* of $r_{e,est}$
$\boldsymbol{S}$	S_{est} +10	S_{est} - 10

3.9.2 - CONFIDENCE INTERVAL

This is a statistical interval estimate of a model parameter used to indicate the reliability of the parameter estimate. This information is not available in traditional graphical well test analysis. Hence matching a wrong reservoir model for a given set of data would give confidence intervals that are not acceptable for most or all the estimates (***Horne***, ***1995***). Also if the data over a given flow regime is missing, this results in a wider confidence interval. Even with an appropriate model, noisy data can also result in a wider confidence interval. TABLE 3.9.2 shows the acceptable confidence ranges based on match of pressure. Roughly twice these values are used when matching pressure derivative.

TABLE 3.9.2: ACCEPTABLE CONFIDENCE LIMITS (Horne, 1995)

Parameter	% Interval	Absolute Interval
$\boldsymbol{K}$	10	-
$\boldsymbol{C_s}$	10	-
$\boldsymbol{\omega}$	20	-
$\boldsymbol{\lambda}$	20	-
$\boldsymbol{r_e}$	10	-

S	-	1.0

The confidence interval of an estimate is a function of noise in the data, the number of data points and the degree of correlation between the unknowns (***Horne***, ***1995***). The procedure used in this work for calculating the confidence intervals of the parameters, ***a***, of a given model, ***p(t$_i$;a)*** are outlined as follows:

1. Calculate the error mean square, ***s$_n^2$***;

$$s_n{}^2 = \frac{SSRn}{n-m} \tag{3.9.24}$$

where:

$$SSRn = \sum_{i=1}^{N} [p_i - p(t_i; a)]^2 \tag{3.9.25}$$

n = number of data points.

m = number of parameters.

2. Evaluate the Hessian matrix , ***H*** defined as given below,

$$H = \begin{bmatrix} \sum_{i=1}^{N} \left(\frac{\partial p}{\partial a_1}\right)\left(\frac{\partial p}{\partial a_1}\right) & \cdots & \sum_{i=1}^{N} \left(\frac{\partial p}{\partial a_1}\right)\left(\frac{\partial p}{\partial a_m}\right) \\ \vdots & \ddots & \vdots \\ \sum_{i=1}^{N} \left(\frac{\partial p}{\partial a_m}\right)\left(\frac{\partial p}{\partial a_1}\right) & \cdots & \sum_{i=1}^{N} \left(\frac{\partial p}{\partial a_m}\right)\left(\frac{\partial p}{\partial a_m}\right) \end{bmatrix} \tag{3.9.26}$$

3. Evaluate the standard error of each parameter, ***σ_{aj}^2***;

$$\sigma_{a_j}^2 = s_n^2 \, H_{jj}^{-1} \tag{3.9.27}$$

H_{jj}^{-1} is the jth diagonal element of the inverse Hessian matrix, evaluated at ***a*** = ***a****

4. A (1 – α) x 100 % confidence interval is evaluated using Equation (3.9.28).

$$a_j^* - \sigma_{a_j} \cdot t_{1-\frac{\alpha}{2}} \le a_j \le a_j^* + \sigma_{a_j} \cdot t_{1-\frac{\alpha}{2}} \tag{3.9.28}$$

Where, for a two tailed distribution, $t_{1-\frac{\alpha}{2}}$ is a tabulated value that cuts off $\frac{\alpha}{2}$ x 100% in the tails of the student ***t – distribution*** with ***n-m*** degrees of freedom. But for large ***n,*** such that the degree of freedom, ***n-m***, is greater than 30, the t-distribution approaches a normal distribution. Therefore using a ***95%*** confidence interval, i.e. α = 5, the corresponding value of the normal distribution is 1.96. Hence, the confidence interval of each parameter is computed as using Equation (3.9.29).

$$a_j^* - 1.96 \cdot \sigma_{a_j} \le a_j \le a_j^* + 1.96 \cdot \sigma_{a_j} \tag{3.9.29}$$

However, a confidence interval does not predict that the true value of the parameter has a particular probability of being in the confidence interval given the data actually obtained.

Conclusions

A computer-aided approach to well test interpretation has been presented in this work. Although this approach is limited to eight fundamental reservoir models (***Anraku***, ***199),*** it aims to completely automate the well test

interpretation procedure. Also, this work intends to highlight the following benefits of automating well test analysis;

1. For better accuracy, as this will avert the subjective results of well test analysis.
2. For real time monitoring; this will be an added value to the invention of permanent down-hole gauges and recent developments in computer technology. With a computer aided well test analysis, the vast amount of data obtained can be analyzed in a short time, producing reliable results.
3. Although good engineering judgment cannot be replaced by the use of computers, the importance of automating well test analysis stems from the fact that it presents a quantitative means of comparing different results.

In the part 2 of this paper, this approach is implemented in a computer program; WELL TEST AUTO. The analysis of the results of well test data used to validate this approach is also presented in the second part of this paper.

References

Abramowitz, M. and ***Stegun, I.A.*** (***1964***): "*Handbook of Mathematical Functions*", Applied Mathematics Series, Volume 55 Washington, National Bureau of Standards; reprinted 1968 by Dover Publications, New York.

Al-Kaabi, ***A. U***. and ***Lee, W. J.*** (***1990***): "*Using Artificial Neural Networks to Identify the Well Test Interpretation Model*", paper SPE 20332 presented at the 1990 5th SPE Petroleum Computer Conference, Denver, Colorado,June 25-28.

Allain, O. F. (***1987***): "*AN ARTIFICIAL INTELLIGENCE APPROACH TO WELL TEST*" M.Sc Report, Stanford University.

Allain, O. F. and ***Houźe O.P.*** (***1992***): "*A Practical Artificial Intelligence Application in Well Test Interpretation*", paper SPE 24287 presented at the 1992 SPE European Petroleum Computer Conference, Stavanger, Norway, May 25-27.

Allain, O. F. and ***Horne, R. N.*** (***1990***): "*Use of Artificial Intelligence in Well Test Interpretation*", J. Petroleum Tech., (March 1990), pp 342 – 349.

Anraku, T. (***1993***): "*DISCRIMINATION BETWEEN RESERVOIR MODELS IN WELL TEST ANALYSIS*", Ph.D Dissertation, Stanford Univeristy.

Anraku, T. and ***Horne, R. N.*** (***1995***): "*Discrimination Between Reservoir Models in Well Test Analysis*", SPE Formation Evaluation, (June), pp 114-121.

Athichanagorn, S. and ***Horne, R. N.*** (***1995***): "*Automated Parameter Estimation of Well Test Data using Artificial Neural Networks*", SPE 30556, presented at the 70th Annual Technical Conference and Exhibition, Dallas, TX, October 22-25.

Bariş, G., Horne, R. N. and ***Eric T.*** (***2001***): "*Automated Reservoir Model Selection in Well Test Interpretation*", paper SPE 71569, presented at the 2001 SPE Annual Technical Conference and Exhibition, held in New Orleans, Louisiana, U.S.A., September 30 to October 3.

Bourdet, D. (***2002***): "*WELL TEST ANALYSIS: THE USE OF ADVANCED INTERPRETATION MODELS*" – (Handbook of Petroleum Exploration and Production, 3), First Edition, Elsevier Science Publishing Co. Amsterdam, The Netherlands.

Bourdet, D., Ayoub, J. A. and Pirard, Y. M. (***1989***): "*Use of Pressure Derivative in Well-Test Interpretation*", SPE Formation Evaluation, pp. 293-302.

Bourdet, D., Whittle T.M., Douglas, A.A. and Pirard, Y-M. (***1983a***): "*A New Set of Type Curves Simplifies Well Test Analysis*", World Oil, Vol. 196, No. 6.

Bourdet, D., Whittle, T.M., Douglas, A.A. Pirard, Y.M. and Kniazeff, V.J. (***1983b***): "*Interpreting Well Tests in Fractured Reservoirs*", World Oil (October) 95-106.

Dastan, A. and ***R. N. Horne*** (***2011***): "*Robust Well-Test Interpretation by Using Nonlinear Regression With Parameter and Data Transformation*", SPE Journal, doi: 10.2118/132467-PA.

Davis, E. G. Jr. and ***Hawkins, M. F. Jr.*** (***1963***): "*Linear Fluid-Barrier Detection by well measurements*", SPE Journal of Petroleum Technology (October), Vol. 15, Number 10.

Earlougher, R. C. Jnr. (***1977***): "*Advances in Well Test Analysis*", Second Printing, American Institute of Mining, Metallurgical, and Petroleum Engineers, Inc. Millet the Printer, Inc.

Ershaghi, I., Li, X., and Hassibi, M. (***1993***): "*A Robust Neural Network Model for Pattern Recognition of Pressure Transient Test Data*", paper SPE 26427 presented at the 1993 SPE Annual Technical Conference and Exhibition, Houston, Texas, October 3-6.

Gray, K. E. (***1965***): "*Approximating Well-to-Fault Distance from Pressure Build-Up tests*", SPE Journal of Petroleum Technology (July), Vol. 17, Number 7.

Gringarten, A. C. (***2008***): "*From Straight Lines to Deconvolution: The Evaluation of the State of the Art in Well Test Analysis*", SPE102079, SPE Reservoir Evaluation & Engineering, pp 41-62 February 2008

Gringarten, A. C., Bourdet, D. P., Landel, P. A. and ***Kniazeff, V. J. (1979***): "*A Comparison Between Different Skin and Wellbore Storage Type-Curves for Early-Time Transient Analysis*", paper SPE 8205, presented at the SPE Annual Technical Conference and Exhibition, Las Vegas, Nevada.

Horne, R. N. (***1995***): "*Modern Well Test Analysis: A Computer-Aided Approach*", Petroway, Inc., Palo Alto, CA, Second Edition 1995.

Horne, R. N. (***1994***): "*Advances in Computer-aided Well Test Interpretation*", Journal of Petroleum Technology, (46) 7 pp. 599-606 1994.

Lee, J. (***1982***): "*Well Testing",* Dallas, TX: Society of Petroleum Engineers of the AIME.

Marquardt, D. W. (***1963***): "*An Algorithm for Least-squares Estimation of Nonlinear Parameters*", Journal of the Society for Industrial and Applied Mathematics, vol. 11, (SIAM J). pp. 431-441.

Onyekonwu, M. O. (***1997***): "*GENERAL PRINCIPLES OF BOTTOM-HOLE PRESSURE TESTS",* Laser Engineering Consultants, Port Harcourt, Nigeria.

Press, W. H., Teukolsky, S. A., Vetterling, W. T. and ***Flannery, B. P.*** (***2007***): "*Numerical Recipes in C, The Art of Scientific Computing*", Second Edition, Cambridge University Press.

Ramey, H. J. (***1970***): "*Short-Time Well Test Data Interpretation in the Presence of Skin Effect and Wellbore Storage*", Journal of Petroleum Technology 22 (1) pp. 97-104.

Rosa, A. J. and ***Horne, R.N.*** (***1983***): "*Automated Type Curve Matching in Well Test Analysis Using Laplace Space Determination of Parameter Gradients*", paper SPE 12131, presented at the 1983 SPE Annual Technical Conference, San Francisco.

Stehfest, H. (***1970***): "*Algorithm 368: Numerical inversion of Laplace transforms*", Comm. ACM. 13:47–49.

Von Schroeter, T., Hollaender, F. and ***Gringarten, A. C.*** (***2001***): "*Deconvolution of Well Test Data as a Nonlinear Total Least Squares Problem*", paper SPE 71574 presented at the 2001 SPE Annual Technical Conference and Exhibition New Orleans, Louisiana.